2009

A Model for Coupled Electrical Migration and Stress-Driven Transport in Anodic Oxide Films

Kurt R. Hebert
Iowa State University, krhebert@iastate.edu

Jerrod E. Houser
Iowa State University

A Model for Coupled Electrical Migration and Stress-Driven Transport in Anodic Oxide Films

Abstract
A model for transport in amorphous anodic oxide films was developed in which ion migration was driven by gradients of mechanical stress as well as electric potential and which included viscoelastic creep of the oxide. Simulations were presented for the galvanostatic growth of planar barrier-type anodic aluminum oxide films. It is assumed that stress originates at the metal-film interface due to the volume change upon oxidation. The average stress in the film decayed during growth and evolved from compressive to tensile with increasing applied current density. The model was fit to stress-thickness measurements using a viscosity of 1×1012Pas on the same order of magnitude as that of many other amorphous materials displaying viscous creep. The current density increased exponentially with electric field, in agreement with an empirical high field conduction behavior. The metal ion transport number was predicted based on the motion of markers in the film and increased with current density in quantitative agreement with experimental measurements. The model represents a unified quantitative interpretation of ionic conduction, transport numbers, and mechanical stress measurements in anodic films.

Keywords
aluminum compounds, anodisation, creep, electric potential, viscosity

Disciplines
Chemical Engineering

Comments
This article is from *Journal of the Electrochemical Society* 156 (2009): C275–C281, doi:10.1149/1.3151835.
Posted with permission.

Journal of The Electrochemical Society, **156** (8) C275-C281 (2009)
0013-4651/2009/156(8)/C275/7/$25.00 © The Electrochemical Society

A Model for Coupled Electrical Migration and Stress-Driven Transport in Anodic Oxide Films

Kurt R. Hebert[*,z] **and Jerrod E. Houser**[**]

Department of Chemical and Biological Engineering, Iowa State University, Ames, Iowa 50014, USA

A model for transport in amorphous anodic oxide films was developed in which ion migration was driven by gradients of mechanical stress as well as electric potential and which included viscoelastic creep of the oxide. Simulations were presented for the galvanostatic growth of planar barrier-type anodic aluminum oxide films. It is assumed that stress originates at the metal-film interface due to the volume change upon oxidation. The average stress in the film decayed during growth and evolved from compressive to tensile with increasing applied current density. The model was fit to stress-thickness measurements using a viscosity of 1×10^{12} Pa s on the same order of magnitude as that of many other amorphous materials displaying viscous creep. The current density increased exponentially with electric field, in agreement with an empirical high field conduction behavior. The metal ion transport number was predicted based on the motion of markers in the film and increased with current density in quantitative agreement with experimental measurements. The model represents a unified quantitative interpretation of ionic conduction, transport numbers, and mechanical stress measurements in anodic films.
 [DOI: 10.1149/1.3151835]

Manuscript submitted December 9, 2008; revised manuscript received May 5, 2009. Published June 22, 2009.

Recent experimental evidence suggests that plastic flow of oxide occurs during the growth of anodic oxide films and contributes significantly to ionic mass transport. Skeldon and co-workers used tungsten tracers introduced from the metal to visualize ionic transport within porous anodic alumina films formed in acidic solutions.[1-4] The observed tracer motion deviated strongly from expectations based on electrical migration as the only transport mechanism, the authors attributing the discrepancy to plastic flow in the oxide. The tracer studies supported earlier measurements of the rate of increase in pore wall height relative to stationary reference planes.[5-7] Both experiments revealed plastic flow in the pore walls at typical velocities of 0.1–1 nm/s. We developed a transport model of porous anodic alumina films, which validated the hypothesis of coupled electrical migration and viscous flow of oxide, through a detailed agreement with the tungsten tracer profiles.[8] The results of this study suggest that the coupled stress and potential distributions in these films regulate the interface motion during the formation of self-ordered pore arrays.

The importance of viscous creep may extend beyond porous oxides to planar anodic films typically formed in neutral pH solutions. Evidence for creep in such films is suggested by several experimental studies. Leach and co-workers observed a current-dependent extension of loaded Al wires during anodizing, which they attributed to current-induced plasticity in the anodic film.[9,10] Wüthrich showed that anodic alumina films deform without cracking during anodizing.[11] Zhou et al. attributed the observations of growth and coalescence of oxygen bubbles during the passage of ionic current to the plasticity in the surrounding oxide.[12,13] An additional precedent for creep of amorphous solids at ambient temperatures is found in studies that show that Newtonian viscous flow relieves compressive stresses induced by ion irradiation.[14-17] Like the materials in these experiments, anodic alumina films are amorphous, and stresses large enough to drive significant creep (10–100 MPa) are found during the growth of both porous and planar anodic alumina.[9,11,18-21] Stresses during anodizing may arise from volume constraints at the metal–oxide interface, and from electrostatic forces in the oxide dielectric.[22-24]

In this paper, we present a model for transport in planar anodic films by coupled electrical migration, plastic flow, and migration in the stress field. Coupling of transport processes results from the constraints of volume and charge conservation. The model is developed for the specific case of barrier-type aluminum oxide films, which have been studied extensively. However, a similar treatment may apply to amorphous anodic oxides formed on a variety of valve metals. The model is adapted from the continuum approach developed by Suo and co-workers to model coupled plastic flow and diffusional transport in metals.[25,26] The calculated results are compared to stress measurements, current–electric field relations, and marker studies yielding metal ion transport numbers. An encouraging agreement is found with all three types of experimental measurements, suggesting that the model may provide a unified framework for understanding transport in anodic films.

Model

The model approximates the anodic film as a homogeneous Al_2O_3 continuum with uniform properties. The concentrations of current-carrying defects are assumed to be constant and proportional to the concentrations of the metal and oxygen ions. The mass density is taken to be constant in view of the much larger elastic modulus of alumina ($\sim$100 GPa [27]) relative to typical anodizing stresses (10–100 MPa). These values imply that the in-plane elastic strain is small, and hence the density may be considered constant. Direct measurements of the density reveal that it is independent of anodizing current density.[28]

Stress gradients can produce transport by both creep and migration of chemical species.[25,26] To account for stress migration, the empirical high field conduction relation is generalized by considering the driving force for migration to be the gradient of the ionic chemical potential μ_i

$$J_i = -C_i u_i^0 \sinh\left(\frac{a}{RT}\frac{\partial \mu_i}{\partial z}\right) \quad [1]$$

where J_i, C_i, and u_i^0 are respectively, the flux, the concentration, and the pre-exponential velocity of ion "i," and a is the migration jump distance in the oxide. All gradients are one-dimensional and depend only on the z-coordinate, which extends perpendicular to the film interfaces. The use of chemical potential gradients in high field conduction was introduced by Battaglia and Newman, who obtained rate equations in the presence of combined concentration gradients and electric fields.[29] In the present model, the ionic concentrations are uniform, but there are contributions to μ_i from both electrical potential and stress

$$\mu_i = \mu_i^0 + z_i F\phi - \bar{V}_i\sigma \quad [2]$$

where μ_i^0, z_i, and $\bar{V}_i$ are the standard chemical potential, the charge number, and the molar volume of ion i, respectively, and ϕ is the electric potential. σ is the mean stress, i.e., the average of σ_{xx}, σ_{yy}, and σ_{zz}, and is equivalent to the negative pressure. For planar oxide films, the stress in the oxide is biaxial, with equal nonzero components parallel to the interface and a zero normal stress component.

* Electrochemical Society Active Member.
** Electrochemical Society Student Member.
z E-mail: krhebert@iastate.edu

The z-direction normal stress is zero because the solution-phase pressure opposing σ_{zz} is negligible relative to the stresses in the anodic film. The model equations are written in terms of σ_{xx} because experiments measure this stress component averaged through the film thickness, and the sign convention is adopted that σ_{xx} is positive if tensile and negative if compressive. Using μ_i from Eq. 2 in Eq. 1 yields the flux equation

$$J_i = C_i u_i^0 \sinh\left[\frac{a}{RT}\left(z_i F E_z + \frac{2}{3}\bar{V}_i \frac{\partial \sigma_{xx}}{\partial z}\right)\right] \quad [3]$$

where E_z is the electric field in the z direction. The subscript i is M for metal ions and O for oxygen ions. A flux perpendicular to the metal–film interface would result from a gradient of σ_{xx} in this direction even though the stress component perpendicular to the interface, σ_{zz}, is zero.

The anodic oxide film composition is stoichiometric Al_2O_3. According to the ionic radii of Al^{+3} and O^{-2}, 0.039 and 0.14 nm, respectively,[30] Al^{+3} accounts for only 1.4% of the occupied volume of Al_2O_3. For simplicity, we therefore approximate the metal ions as point charges by setting $\bar{V}_M$ in Eq. 3 to zero; thus, the transport of only oxygen and not metal ions contributes to the volume flux in the film. The oxygen ion concentration is $C_O = 1/\bar{V}_O$, and the metal ion concentration is determined by electrical neutrality, $C_M = 2/(3\bar{V}_O)$. According to Eq. 3, the electrical migration of the trivalent metal ions increases faster with electric field than that of the divalent oxygen ions. As the ionic current and electric field increase, a greater share of the current is carried by the Al^{+3} point charges; therefore, the volume per unit conducted charge in the film becomes smaller. Below we show that this principle underlies the dependence of stress on applied current density.

The model enforces electrical charge and volume conservation and the momentum balance in a Newtonian fluid. The former requirement may be written simply as

$$i = -2FJ_O + 3FJ_M \quad [4]$$

where i is the applied current density. The uniform current density through the film thickness implies that any space-charge distribution is at steady state. The volume balance is

$$\frac{i\Omega_M}{3F} = -\bar{V}_O J_O - v_z \quad [5]$$

where Ω_M is the molar volume of Al atoms in the metal and v_z is the creep velocity in the oxide. Equation 5 states that the volume rate of metal consumption by oxidation balances the flux in the oxide due to O^{-2} migration and plastic flow. The charge and volume balances are equivalent to species balances for metal and oxygen ions. To model plastic flow, we apply the Maxwell viscoelastic model, which was used successfully to describe the viscous relaxation of amorphous materials in ion beams[14]

$$0 = \frac{\sigma_{xx}}{6\eta} + \frac{1}{3}\frac{\partial v_z}{\partial z} + \frac{1}{Y}\frac{\partial \sigma_{xx}}{\partial t} \quad [6]$$

Here, η is the viscosity and Y is the elastic modulus. Equation 6 reduces to the momentum balance in a Newtonian fluid when the elastic modulus is very large. Amorphous SiO_2 films formed by thermal oxidation exhibit plasticity; i.e., their viscosity decreases dramatically above a critical stress.[31,32] We take the viscosity of anodic alumina to be constant but incorporate plasticity through the boundary condition at the metal–film interface, as described below.

In addition to the viscoelastic stress in Eq. 6, experimental measurements incorporate the electrostatic stress, σ_{xx}^{ES}, that is the sum of the Maxwell and electrostriction stresses in the dielectric film. Recently, Vanhumbeeck and Proost[24] showed that measurements of σ_{xx}^{ES} in anodic TiO_2 obeyed an expression derived by Shkel and Klingenberg.[33] Using this model, the correction for electrostatic stress is

$$\sigma_{xx}^{exp} = \sigma_{xx} + \sigma_{xx}^{ES} = \sigma_{xx} + \frac{\epsilon_0(K + a_2)}{2}E_z^2 \quad [7]$$

where the average of σ_{xx}^{exp} through the film thickness is the experimentally measured stress, ϵ_0 is the permittivity of free space, K is the dielectric constant of the anodic oxide, 8.4,[28] and the K-dependent constant a_2 has the value of −18.3 for alumina.[24] With the nearly uniform electric fields present in the oxide during high field conduction, the electrostatic stress is a uniform compressive contribution to the in-plane stress σ_{xx}. At typical electric fields of 0.8 V/nm during anodizing, σ_{xx}^{ES} is approximately −30 MPa. The electrostatic stress is assumed to be constant here.

The domain of the model is bounded by the metal–film interface $[z = z_1(t)]$ and the film–solution interface $[z = z_2(t)]$. These boundaries move with time as metal is consumed and the film thickness increases. A reduced spatial coordinate, $\zeta = [z - z_1(t)]/h(t)$, is adopted, where $h(t) = z_1(t) - z_2(t)$ represents the oxide film thickness. In the neutral pH range where planar anodic film growth occurs, there is no significant metal dissolution at the film–solution interface; i.e., the current efficiency for film growth is approximately 100%. Therefore, the film thickness increases linearly with time according to

$$h(t) = h_0 + \frac{i\bar{V}_0}{2F}t \quad [8]$$

The model equations were converted to the dimensionless scaled variables $v = v_z/v_I$, $\varepsilon = E_z/E_z^\star$, $s = \sigma_{xx}/\sigma^\star$, and $\tau = t/t^\star$. The velocity and stress scales were chosen as $v_I = i\Omega_M/3F$, the metal–film interface velocity, and $\sigma^\star = (2\eta v_I)/\lambda$, the scale associated with the viscous stress, as derived from Eq. 6. The length scale is derived from Eq. 3 for the O^{-2} flux

$$\lambda = \left(\frac{4a\eta v_I \bar{V}_O}{3RT}\right)^{1/2} \quad [9]$$

We show below that λ represents the thickness of regions in which significant stress gradients exist. Suo found a similar length scale in his model of coupled creep and self-diffusion in metals.[26] We choose the time scale associated with film growth, $t^\star = \lambda/v_I$, and the electric field scale is $E_z^\star = RT/aF$. In a dimensionless form, the charge, volume, and momentum balances were simplified to obtain

$$\varepsilon = \frac{1}{3}\sinh^{-1}\left(\frac{\Phi - 1 - v}{\alpha_M}\right) \quad [10]$$

$$\frac{\partial s}{\partial \zeta} = (\delta_0 + \Phi\tau)\left[\frac{2}{3}\sinh^{-1}\left(\frac{\Phi - 1 - v}{\alpha_M}\right) - \sinh^{-1}\left(\frac{v + 1}{\alpha_O}\right)\right] \quad [11]$$

$$0 = (\delta_0 + \Phi\tau)\left(\beta\frac{\partial s}{\partial \tau} + s\right) + \frac{\partial v}{\partial \zeta} - \beta(\Phi\zeta - 1)\frac{\partial s}{\partial \zeta} \quad [12]$$

The dimensionless parameters in these equations are defined as $\alpha_M = u_M^0/v_I$, $\alpha_O = u_O^0/v_I$, $\beta = 6\eta/Yt^\star$, and $\delta_0 = h_0/\lambda$. Φ is the Pilling–Bedworth ratio, $3\bar{V}_O/2\Omega_M$, the ratio of the volume of Al_2O_3 formed by oxidation to that of Al consumed. α_M and α_O, which are ratios of the pre-exponential migration velocities to the interfacial velocity, depend on the applied current density. β expresses the importance of elastic forces relative to viscous forces.

The boundary condition at the metal–film interface specifies the relative contributions of creep and migration to the motion of the oxide at the interface. When the magnitude of the interfacial stress is relatively small, we assume that the oxide motion is entirely by migration and therefore use the boundary condition $v = 0$ at $\zeta = 0$. When this boundary condition is used at all current densities, the model predicts large compressive and tensile interfacial stresses at small and large currents, respectively. In some simulations, we in-

corporated the effect of interfacial oxide plasticity, as inferred by Leach from observations of the relaxation of Al wires under loads during anodic oxidation at high current densities.[9,10] Our approach to simulate plasticity is based on models of the thermal oxidation of silicon, in which the viscosity of SiO_2 is dramatically decreased above a threshold stress.[31,32,34] Because the enhanced fluidity of the oxide would facilitate creep at the interface, we simply imposed a limiting critical stress at the metal–oxide interface, at which further increases in the creep rate would require negligible additional stress.[35] The zero-velocity boundary condition is used only when the calculated interfacial stress is between the compressive and tensile limits, $\sigma_{xx}^{\min}$ and $\sigma_{xx}^{\max}$. At lower current densities, the boundary condition is $\sigma_{xx} = \sigma_{xx}^{\min}$, and at higher current densities, $\sigma_{xx} = \sigma_{xx}^{\max}$. The additional boundary condition was $\sigma_{xx} = 0$ at $\zeta = 1$ because the oxide deposited at the film–solution interface is assumed to be free of viscoelastic stress. Because the calculations were found to be insensitive to the initial conditions, it was assumed for simplicity that the stress in the native oxide film is zero.

Results and Discussion

Experimental stress measurements.— Several papers report stress measurements during the growth of anodic alumina films, but unfortunately there is a disagreement on several aspects of experimental phenomena.[9,11,18,21] Both Vermilyea and Bradhurst observed transitions from compressive to tensile stress with increasing current density. Other studies of porous anodic alumina growth found the same trend.[19,20] Two papers cited similar current densities of about 0.6–1 mA/cm^2 at the transition.[9,19] However, Wüthrich, using a different experimental technique, found only compressive growth stresses, which increased in magnitude with current density.[11] Several studies agree that the stress shifts in the tensile direction upon turning off the anodizing current, but while Bradhurst and Nelson found shifts corresponding to the expected electrostatic stress, those observed by Vermilyea and Wüthrich were appreciably larger. None of these studies reported the time dependence of the tensile shift, which is relevant to its possible assignment to electrostatic stress.[24] As shown below, a compressive to tensile transition with increasing current density is intrinsic to the behavior of the present model. Therefore, we compare our calculations to the measurements of Bradhurst and Leach,[9,21] who found this trend and also characterized the dependence of stress on oxide thickness and current density. Like these authors, we attribute the difference between the growth stress and the stress at open circuit to electrostatic stress. Hence, we present calculations of σ_{xx} (not $\sigma_{xx}^{\exp}$) and compare these to the experimental stress at open circuit. Because stress in the present model derives from oxide formation at the metal–film interface, the disagreement between Bradhurst and others may be due to additional sources of stress at the film–solution interface, which did not contribute significantly to Bradhurst's experiments.

General features of model behavior.— In this section, results are presented, illustrating the evolution of oxide stress and creep during film growth. The calculations here and elsewhere in the paper used ion migration parameters based on the current density at the transition from compressive to tensile stress, which was taken to be 0.6 mA/cm^2.[9,19] Because both the stress gradient and the creep velocity are zero at this current density, the ionic fluxes J_M and J_O could be determined separately from Eq. 4 and 5. Also, the slope $d \ln i/dE$ was evaluated at the stress-free current density from Eq. 3 and 4. Experimental values of both the electric field and $d \ln i/dE$ at 0.6 mA/cm^2 are known from a study of anodic film growth.[36] The conduction parameters were then determined by applying these values in the expressions for J_M, J_O, and $d \ln i/dE$. In this way, the parameters $u_O^0 = 1.20 \times 10^{-17}$ cm/s, $u_M^0 = 1.31 \times 10^{-22}$ cm/s, and $a = 0.370$ nm were obtained.

Figure 1 displays examples of dimensionless stress transients during oxide growth for three representative current densities. These calculations did not use limiting interfacial stress, and instead the zero-velocity boundary condition was applied at each current density. The current density of 0.3 mA/cm^2 results in compressive stress because it is below the zero-stress current density of 0.6 mA/cm^2; the other two current densities produced tensile stress because they are higher than the critical value. Each transient has a maximum compressive or tensile stress at a dimensionless time $\tau \approx 0.5$–0.7, followed by a decay over time $\tau \approx 5$. The dimensionless time is directly related to the extent of film growth $\Delta h = h(t) - h_0$, i.e., $\tau = \Delta h/\Phi\lambda$, where $\Phi = 1.65$. Thus, the stress maxima correspond to $\Delta h \approx \lambda$, and the decay times correspond to $\Delta h \approx 8\lambda$.

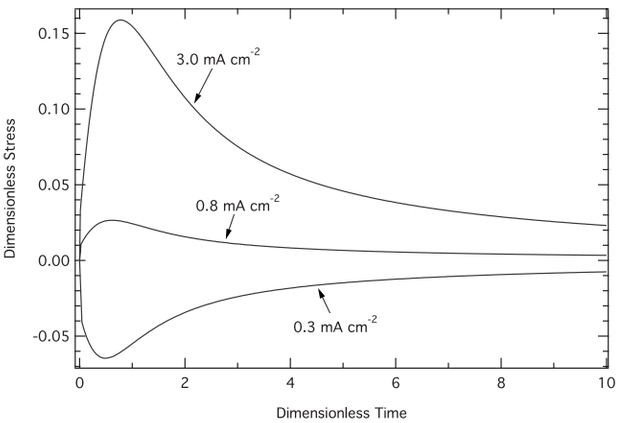

Figure 1. Variation in dimensionless stress with dimensionless time at three selected current densities. The velocity was set to zero at the metal–film interface.

The stress and velocity profiles in Fig. 2 clarify the relationship between the stress transients and the characteristic length λ. Profiles are shown for τ values of 1 and 3 at the current density of 3.0 mA/cm^2. Again, the zero-velocity boundary condition was applied at the metal–film interface. Both stress and velocity profiles are nearly the same for the two film thicknesses, each profile decaying to a constant value over a distance of $z/\lambda \approx 2$. Because the velocity is zero at the metal–film interface, an interfacial stress gradient is required to adjust the rate of O^{-2} migration J_O to satisfy the volume balance. The contribution of J_O to the volume balance becomes smaller with distance from the metal as the stress gradient relaxes and the creep velocity increases. At the distance of $z \approx 2\lambda$ the stress has decayed significantly, and the volume balance is satisfied primarily by electrical migration and plastic flow. The maxima in Fig. 1 can therefore be understood as follows: At times smaller than the maxima, the overall film thickness h is smaller than λ, and so a relatively small interfacial stress is needed to supply the required stress gradient. At times after the maxima, h is larger than λ.

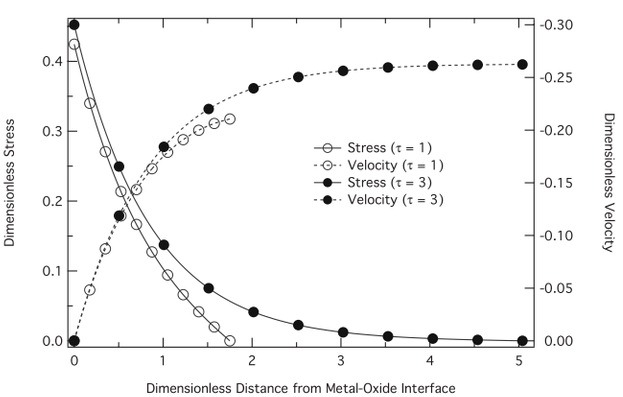

Figure 2. Calculated dimensionless stress and creep velocity profiles in anodic films for two selected times during anodizing at 3 mA/cm^2.

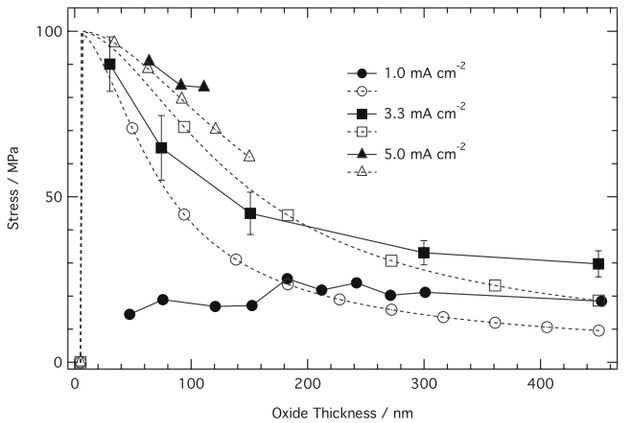

Figure 3. Comparison of model calculations with measurements of stress variation with anodic film thickness (tensile regime). Solid markers are stress measurements after the interruption of anodizing at current densities of 1.0 and 5.5 mA/cm^2 [21] and 3.3 mA/cm^2.[9] The vertical bars at 3.3 mA/cm^2 represent the variability of stress with repeated measurements. The dashed curves and open markers are model calculations. Model parameters: Viscosity $\eta = 1 \times 10^{12}$ Pa s and maximum interfacial stress $\sigma_{xx}^{max} = 200$ MPa.

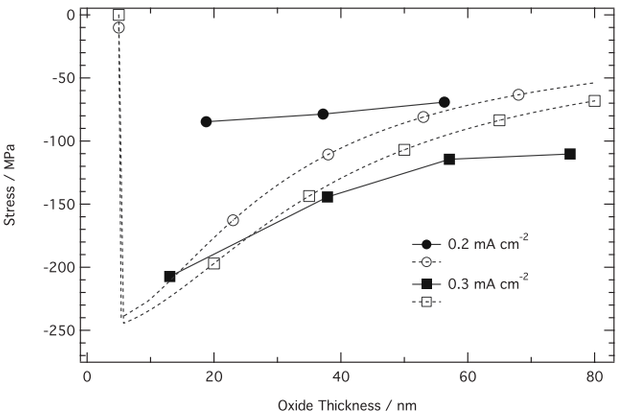

Figure 4. Comparison of model calculations with measurements of stress variation with anodic film thickness (compressive regime). Solid markers are stress measurements after interruption of anodizing at current densities of 0.2, 0.3, and 0.4 mA/cm^2.[21] The dashed curves and open markers are model calculations. Model parameters: Viscosity $\eta = 1 \times 10^{12}$ Pa s and minimum interfacial stress $\sigma_{xx}^{min} = -500$ MPa.

The stress and velocity profiles remain the same, but the average stress is reduced by the contribution of the stress-free outer region of the film. The transient stress response is sensitive to parameters that determine λ; in particular, Eq. 9 indicates that λ is proportional to the square roots of the viscosity and current density.

The calculations in Fig. 1 exhibit the experimentally documented transition from compressive to tensile stress with increasing current density.[9,19] This transition is due to the greater sensitivity to electric field of the migration flux of cations relative to anions because of the greater charge of Al^{+3}. At a low current density, the electrical migration of O^{-2} ions dominates because of their high pre-exponential migration velocity. The volume flux to the interface due to the electrical migration of O^{-2} would exceed the generation of free volume by metal oxidation. Accordingly, a compressive stress arises at the interface, which, according to Eq. 2, raises the chemical potential of oxygen ions and hence reduces the flux of O^{-2}. As the current density and electric field become larger, the electrical migration of the trivalent Al^{+3} ion increases more rapidly than that of the divalent O^{-2} ions. Eventually, the volume flux due to electrical migration would be insufficient to fill the reacted volume of metal, and a tensile stress develops at the interface, which reduces the O^{-2} chemical potential, consequently enhancing the oxygen flux. Bradhurst and Leach[9] and Nelson and Oriani[19] both explained the compressive–tensile transition qualitatively in terms of the increase with electric field of the ratio of metal to oxygen migration rates. Our model exhibits the same behavior, resulting simply from the higher charge of Al^{+3} ions compared to O^{-2} ions.

Comparison of model to stress measurements during anodic oxidation.— In this section, the model is compared to the experiments of Bradhurst and Leach characterizing the dependence of stress on oxide thickness and current density.[9,21] Figures 3 and 4 show stress vs oxide thickness in cases where tensile and compressive stresses, respectively, were observed. The stress decay at 3.3 mA/cm^2 (Fig. 3) suggests a characteristic length λ of about 50 nm, and that at 0.3 mA/cm^2 (Fig. 4) indicates that λ is approximately 15 nm. Both λ values are consistent with a viscosity of 1×10^{12} Pa s, according to Eq. 9. When this viscosity was used with no limiting interfacial stress, the magnitude of the stress at small film thickness was much larger than the experimental values. To represent the measurements, limiting stress boundary conditions were used in both Fig. 3 and 4, with $\sigma_{xx}^{min} = -500$ MPa and $\sigma_{xx}^{max} = 200$ MPa. The sharp increases of the calculated stress at zero film thickness result from the artificial initiation condition of zero stress used in the simulation. While the magnitude of the predicted stress in all cases decayed with oxide thickness, in some of the measurements (i.e., 5.0 and 0.2 mA/cm^2) the stress was relatively independent of thickness. The reason for the experimental variability is not clear. Nonetheless, the results in Fig. 3 and 4 indicate that the model successfully follows the overall dependence of the stress transients on current density. The parameter β is 0.1–0.3 for the simulations in Fig. 3 and 4, indicating a relatively small effect of elasticity on the results.

The fit model parameters correspond well with values of other materials undergoing plastic flow. The viscosity of 1×10^{12} Pa s is particularly noteworthy because viscosities of the same magnitude are found in many studies of the viscous flow of amorphous materials. These include ion-irradiated viscous materials at ambient temperature[15] and SiO_2 films during thermal oxidation of Si.[37] The limiting stress of 200–500 MPa is similar to stresses of 100–500 MPa at which SiO_2 films display significant plasticity.[34] However, it is not clear whether other materials exhibit plasticity at high stresses in both the compressive and tensile directions. Molecular dynamics simulations of creep in amorphous metals show that the plasticity is strongly enhanced by the presence of both vacancy- and interstitial-like defects.[17] It may be possible that a high stress, whether compressive or tensile, stabilizes defects that promote plastic flow in the interfacial region.

Bradhurst and Leach carried out several experiments to fully describe the influence of current density on stress. These measurements are shown in Fig. 5, along with corresponding model predictions. The vertical bars on the data markers represent the variability of stress measurements with oxide thickness over the range of 50–300 nm. The measurements are appreciably scattered but nonetheless display a compressive to tensile transition at 0.5–1.0 mA/cm^2, along with a limiting stress at high current densities. The results for ammonium borate also suggest a maximum compressive stress at about 0.3 mA/cm^2. The calculations used the same values of viscosity and limiting stress as in Fig. 3 and 4, and the plotted results correspond to the same film thickness of 150 nm at all current densities. The zero-velocity boundary condition, when applied at all current densities, gives unrealistically high stress values that increase without bound in the tensile region. The calculations using the same values of σ_{xx}^{max} and σ_{xx}^{max} as in Fig. 3 and 4 showed the correct limiting behavior in the tensile region.

Both sets of calculations also indicated a maximum compressive stress, in agreement with the experimental trend. This feature arises directly from the coupling of stress and electrical migration. At cur-

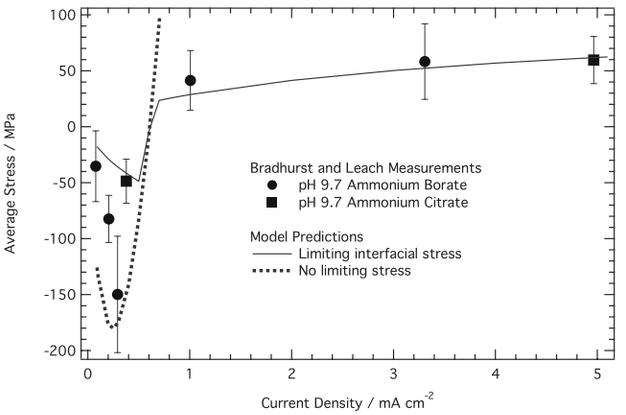

Figure 5. Dependence of stress in anodic films on current density. Markers are stress measurements after current interruptions, and vertical bars represent the variability of stress with oxide thickness over a range to 15–300 nm.[9] Curves are model calculations with no limiting interfacial stress (dashed line) and with $\sigma_{xx}^{min} = -500$ MPa and $\sigma_{xx}^{max} = 200$ MPa (solid line). The viscosity was 1×10^{12} Pa s.

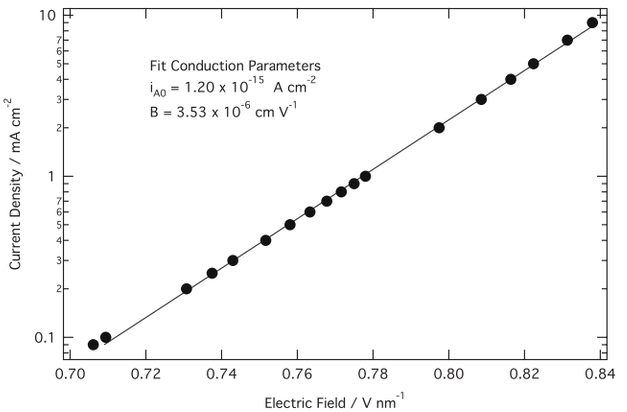

Figure 6. Dependence of anodizing current density on the calculated average electric field in the oxide film. The markers are model results, and the solid line is a linear regression fit. At a given current density, film thicknesses of 50–450 nm yielded the same electric field to three significant digits. The model parameters were the same as those used to calculate the solid line in Fig. 5.

rent densities smaller than the minimum, essentially all the ionic current is carried by O^{-2} ions, and consequently the compressive stress increases in proportion to the interface velocity. When the current density approaches the compressive maximum, the increasing fraction of the current carried by Al^{+3} ions causes the stress to begin shifting in the tensile direction. The compressive maximum at low current densities, followed by a compressive to tensile transition, is a characteristic feature of the model's behavior, which should be readily detectable in experiments. Further empirical evidence for this trend would constitute strong support in favor of the present model.

Comparison of model with empirical conduction behavior.— Ionic conduction in anodic oxide films is empirically found to obey a high field conduction rate expression in the form

$$i = i_{a0} \exp(BE_z) \qquad [13]$$

where i_{a0} and B are empirical parameters. The mathematical form of the high field rate law is typically justified using concepts from the reaction rate theory; that is, the elementary process of conduction is viewed as the field-assisted transfer of a single ion over an energy barrier between neighboring sites in the film.[38] However, in our model conduction includes independent contributions from both Al^{+3} and O^{-2} migrations, and the latter is driven by stress as well as potential gradients. The single-energy barrier model does not capture this added complexity surrounding conduction. It was therefore important to check the predicted current–field relationship for consistency with experimentally observed conduction behavior. In Fig. 6, the applied current density is shown plotted against the calculated average electric field through the film thickness. The current and field closely follow the simple exponential dependence suggested by Eq. 13 over about two decades of current density variation. The film thickness did not influence the calculated field, which remained constant to within three significant digits when the thickness varied between 50 and 450 nm. There is no appreciable curvature in the figure even though the results span regions above and below the stress-free current density of 0.6 mA/cm^2, where the contributions of Al^{+3} and O^{-2} migration, respectively, should predominate. The parameters i_{a0} and B found by linear regression were 1.2×10^{-15} A/cm^2 and 3.53×10^{-6} cm/V, close to their experimental values of 2.4×10^{-15} A/cm^2 and 3.44×10^{-6} cm/V.[36] Figure 6 therefore demonstrates that the predicted current–field relationship agrees very well with the high field equation, despite the multiple processes contributing to conduction.

Motion of markers in the anodic film.— Oxide flow may be inferred from experiments in which markers revealed the separate contributions of the two interfaces to film growth.[39-42] In these papers, the marker position was reported as the metal ion transport number, t_M, i.e., the distance between the markers and the film–solution interface, as a fraction of the film thickness. The term "transport number" derives from the traditional assumptions that the markers are immobile and that ions are transported entirely by electrical migration. t_M would then be equivalent to the fraction of conduction current carried by metal ions. However, in the present model, markers would move with the creep velocity in the film, $dz_t/dt = v_z$, where z_t is the tracer position with respect to stationary coordinates. In terms of the dimensionless variables, the marker position ζ_M obeys

$$\frac{d\zeta_M}{d\tau} = \frac{1 - \Phi\zeta_M + v}{\delta_0 + \Phi\tau} \qquad [14]$$

where ζ_M is the fractional distance between the markers and the metal–film interface. The metal ion transport number t_M is simply $1 - \zeta_M$.

The evolution of the transport number with film thickness was predicted by numerically integrating Eq. 14 using the velocity distributions $v(\zeta,\tau)$ from the film growth simulations in Fig. 5 incorporating interfacial plasticity (solid line). We assumed for simplicity that the markers are initially located at the metal–film interface. Figure 7 shows the metal ion transport number as a function of oxide thickness for current densities from 0.1 to 10 mA/cm^2. At each current density, t_M decreases at first rapidly up to thicknesses of 30–50 nm and then more slowly. The upward displacement of the t_M curves with higher current density is entirely due to flow: If $v = 0$ in Eq. 14, the result for t_M depends on oxide thickness but not on current density

$$t_M = 1 - \frac{1}{\Phi}\left(1 - \frac{h_0}{h}\right) \qquad [15]$$

Therefore, with no flow, t_M decreases during film growth toward a value determined by the Pilling–Bedworth ratio, $t_M = 1 - 1/\Phi = 0.392$. When flow is considered, t_M is smaller than this value at low current densities because the outward flow of oxide moves the tracers toward the film–solution interface; at high current densities, the inward flow increases t_M. The initial decay of t_M with oxide thickness has not been observed experimentally, possibly because of the significant dispersion of implanted tracer depths.[39]

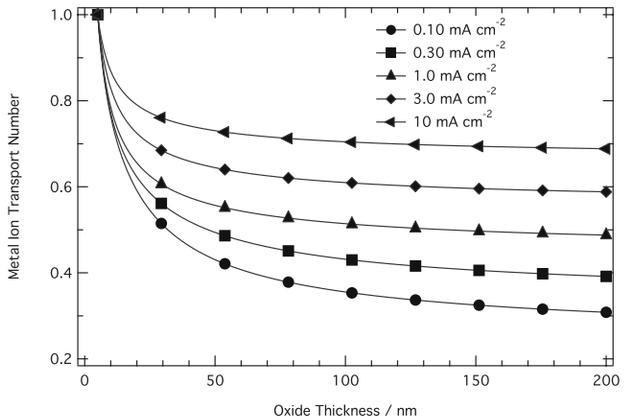

Figure 7. Evolution of predicted marker positions during anodic film growth at the indicated applied current densities. Dependence of anodizing current density on the calculated average electric field in the oxide film. The model parameters were the same as those used to calculate the solid line in Fig. 5.

A direct comparison of transport number measurements with model predictions is shown in Fig. 8 for anodic film thicknesses of 145 nm. Ammonium citrate baths were employed in both the marker experiments[39] and stress measurements used for model parameter fitting (Fig. 5). The solid line in the figure shows the results from Eq. 14 with oxide flow, and the dashed line indicates the constant transport number when the velocity is set to zero. The calculated transport numbers are lower than the measurements, but the model closely follows the data, predicting nearly the same increase in t_M over the current density range. This favorable comparison is important evidence supporting viscous flow in the anodic film because the stress and transport number measurements are entirely independent experiments. The agreement indicates a successful quantitative prediction of marker motion in anodic barrier films. The present concept of stress-driven transport differs significantly from earlier explanations of marker measurements, which were typically based on the cooperative motion of metal and oxygen ions in nanoscale regions.[43,44]

Experimental measurements suggest that the transport-number–current-density relationship depends on the anodizing solution composition. For aqueous phosphate solution, Thompson et al. reported

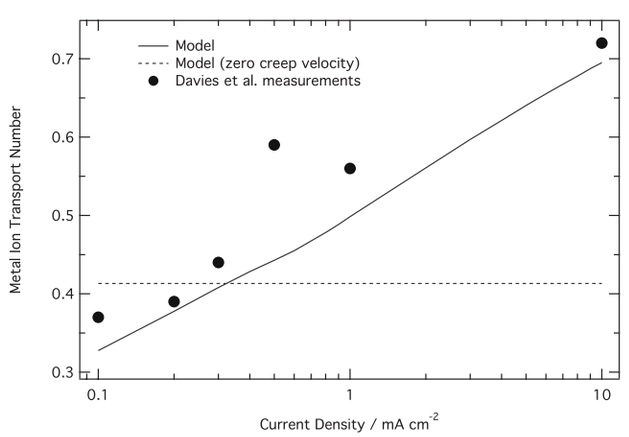

Figure 8. Comparison of model predictions with measurements of Xe^{125} marker positions for anodizing in 3% aqueous ammonium citrate solution.[39] Both experimental data and model predictions correspond to an oxide thickness of 145 nm. The model parameters were the same as those used to calculate the solid line in Fig. 5. The solid curve includes the effect of oxide flow, while the dashed line assumes that the oxide velocity is zero.

a transport number of 0.49 at 1 mA/cm^2, comparable to the results in Fig. 8.[42] In aqueous borate, Khalil and Leach observed a smaller increase in t_M with current density from 0.40 to 0.49 between 6 and 50 mA/cm^2.[41] However, in nonaqueous glycol borate baths, t_M is 0.6–0.7 and does not clearly depend on current density.[39,40] These results indicate that the oxide viscosity and conduction parameters may depend on the solution composition, as a result of electrolyte anion incorporation in the film, typically to levels of several mole percent.[45] We suggest that large anions such as phosphate, citrate, and borate could significantly disrupt the local packing of oxygen ions and influence transport properties by the introduction of additional free volume into the amorphous oxide.[46]

Conclusion

A model for the growth of planar barrier-type anodic oxide films was developed, incorporating the feature that both electrical potential and mechanical stress gradients contribute to ionic transport. In the model, stress and potential gradients combine to drive high field ion migration, and additionally the stress gradient results in viscoelastic creep of the oxide. Stress is generated at the metal-film interface by the volume change upon oxidation. Metal and oxygen ions migrate independently, each at a rate determined by its mobility and electrical charge. Creep and migration are coupled through volume conservation. The model incorporates oxide plasticity by imposing limits on the magnitude of the stress at the metal–oxide interface.

The behavior of the model was demonstrated by simulations of the growth of planar anodic oxide films on aluminum, which are formed in solutions of neutral pH values. Calculations indicate that the stress shifts from compressive to tensile with increasing current density because of the faster migration of trivalent Al^{+3} relative to divalent O^{-2} ions. The local stress decays with distance from the metal–film interface, with an attenuation length proportional to the square roots of the oxide viscosity and current density. Experimentally observed stress decays during the film growth were fit with a consistent viscosity of 1×10^{12} Pa s, which is on the same magnitude as that of other amorphous materials exhibiting viscous flow. Threshold stress values for oxide plasticity were similar to those found during Si oxidation. A maximum compressive stress at low current density was found in both the experiments and model predictions and was associated with the increasing relative importance of cation migration at higher electric fields. Despite the multiple transport processes considered in the model, the current density closely followed a simple exponential dependence on electric field, consistent with empirical high field conduction behavior. The predictions of the dependence of the metal ion transport number on current density agreed quantitatively with experimental measurements. The model thus provides a unified quantitative explanation of conduction, mechanical stress, and marker measurements for anodic films.

Acknowledgments

This research was supported financially by the National Science Foundation (no. DMR-0605957) and by St. Jude Medical Corporation.

Iowa State University assisted in meeting the publication costs of this article.

References

1. P. Skeldon, G. E. Thompson, S. J. Garcia-Vergera, L. Iglesias-Rubianes, and C. E. Blanco-Pinzon, *Electrochem. Solid-State Lett.*, **9**, B47 (2006).
2. S. J. Garcia-Vergara, P. Skeldon, G. E. Thompson, and H. Habazaki, *Electrochim. Acta*, **52**, 681 (2006).
3. S. J. Garcia-Vergara, P. Skeldon, G. E. Thompson, and H. Habazaki, *Appl. Surf. Sci.*, **254**, 1534 (2007).
4. S. J. Garcia-Vergara, P. Skeldon, G. E. Thompson, and H. Habazaki, *Corros. Sci.*, **49**, 3772 (2007).
5. A. P. Li, F. Müller, A. Birner, K. Nielsch, and U. Gösele, *J. Appl. Phys.*, **84**, 6023 (1998).
6. I. Vrublevsky, V. Parkoun, J. Schreckenbach, and G. Marx, *Appl. Surf. Sci.*, **220**, 51 (2003).

7. I. Vrublevsky, V. Parkoun, V. Sokol, J. Schreckenbach, and G. Marx, *Appl. Surf. Sci.*, **222**, 215 (2004).
8. J. E. Houser and K. R. Hebert, *Nature Mater.*, **8**, 415 (2009).
9. D. H. Bradhurst and J. S. L. Leach, *J. Electrochem. Soc.*, **113**, 1245 (1966).
10. J. S. L. Leach and P. Neufeld, *Corros. Sci.*, **9**, 225 (1969).
11. N. Wüthrich, *Electrochim. Acta*, **26**, 1617 (1981).
12. X. Zhou, G. E. Thompson, H. Habazaki, M. A. Paez, K. Shimizu, P. Skeldon, and G. C. Wood, *J. Electrochem. Soc.*, **147**, 1747 (2000).
13. X. Zhou, H. Habazaki, K. Shimizu, P. Skeldon, G. E. Thompson, and G. C. Wood, *Proc. R. Soc. London, Ser. A*, **455**, 385 (1999).
14. C. A. Volkert, *J. Appl. Phys.*, **70**, 3521 (1991).
15. C. A. Volkert and A. Pohlman, *Mater. Res. Soc. Symp. Proc.*, **235**, 3 (1992).
16. T. M. Mayer, E. Chason, and A. J. Howard, *J. Appl. Phys.*, **76**, 1633 (1994).
17. S. G. Mayr, Y. Ashkenazy, K. Albe, and R. S. Averback, *Phys. Rev. Lett.*, **90**, 055505 (2003).
18. D. A. Vermilyea, *J. Electrochem. Soc.*, **110**, 345 (1963).
19. J. C. Nelson and R. A. Oriani, *Corros. Sci.*, **34**, 307 (1993).
20. S. M. Moon and S. I. Pyun, *Electrochim. Acta*, **43**, 3117 (1998).
21. D. H. Bradhurst and J. S. L. Leach, *J. Electrochem. Soc.*, **110**, 1289 (1963).
22. F. H. Stott and A. Atkinson, *Mater. High. Temp.*, **12**, 195 (1994).
23. N. Sato, *Electrochim. Acta*, **16**, 1683 (1971).
24. J. F. Vanhumbeeck and J. Proost, *Colloids Surf., B*, **56**, 163 (2007).
25. Z. Suo, D. V. Kubair, A. G. Evans, D. R. Clarke, and V. K. Tolpygo, *Acta Mater.*, **51**, 959 (2003).
26. Z. Suo, *ASME J. Appl. Mech.*, **71**, 646 (2004).
27. R. S. Alwitt, J. Xu, and R. C. McClung, *J. Electrochem. Soc.*, **140**, 1241 (1993).
28. W. J. Bernard and J. W. Cook, *J. Electrochem. Soc.*, **106**, 643 (1959).
29. V. Battaglia and J. Newman, *J. Electrochem. Soc.*, **142**, 1423 (1995).
30. W. L. Bragg and G. F. Claringbull, *Crystal Structures of Minerals*, Cornell University Press, Ithaca, NY (1965).
31. C. S. Rafferty, L. Borucki, and R. W. Dutton, *Appl. Phys. Lett.*, **54**, 1516 (1989).
32. P. Sutardja and W. G. Oldham, *IEEE Trans. Electron Devices*, **36**, 2415 (1989).
33. Y. M. Shkel and D. J. Klingenberg, *J. Appl. Phys.*, **83**, 7834 (1998).
34. V. Senez, D. Collard, B. Baccus, M. Brault, and J. Lebailly, *J. Appl. Phys.*, **76**, 3285 (1994).
35. J. S. L. Leach and P. Neufeld, *Proc. Br. Ceram. Soc.*, **6**, 49 (1966).
36. A. C. Harkness and L. Young, *Can. J. Chem.*, **44**, 2409 (1966).
37. E. P. Eernisse, *Appl. Phys. Lett.*, **30**, 290 (1977).
38. L. Young, *Anodic Oxide Films*, Academic, London (1961).
39. J. A. Davies, B. Domeij, J. P. S. Pringle, and F. Brown, *J. Electrochem. Soc.*, **112**, 675 (1965).
40. F. Brown and W. D. Mackintosh, *J. Electrochem. Soc.*, **120**, 1096 (1973).
41. N. Khalil and J. S. L. Leach, *Electrochim. Acta*, **31**, 1279 (1986).
42. G. E. Thompson, Y. Xu, P. Skeldon, K. Shimizu, S. H. Han, and G. C. Wood, *Philos. Mag. B*, **55**, 651 (1987).
43. J. P. S. Pringle, *J. Electrochem. Soc.*, **120**, 398 (1973).
44. M.-W. Wang and K. R. Hebert, *J. Electrochem. Soc.*, **146**, 3741 (1999).
45. G. C. Wood, P. Skeldon, G. E. Thompson, and K. Shimizu, *J. Electrochem. Soc.*, **143**, 74 (1996).
46. F. Spaepen, in *Physics of Defects*, R. Balian, M. Kleman, and J.-P. Poirier, Editors, pp. 134–174, North-Holland, Amsterdam (1981).